

# Analyst

Accepted Manuscript



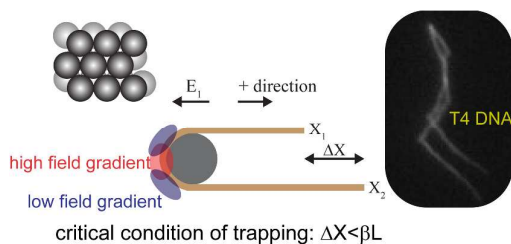
This is an *Accepted Manuscript*, which has been through the Royal Society of Chemistry peer review process and has been accepted for publication.

*Accepted Manuscripts* are published online shortly after acceptance, before technical editing, formatting and proof reading. Using this free service, authors can make their results available to the community, in citable form, before we publish the edited article. We will replace this *Accepted Manuscript* with the edited and formatted *Advance Article* as soon as it is available.

You can find more information about *Accepted Manuscripts* in the [Information for Authors](#).

Please note that technical editing may introduce minor changes to the text and/or graphics, which may alter content. The journal's standard [Terms & Conditions](#) and the [Ethical guidelines](#) still apply. In no event shall the Royal Society of Chemistry be held responsible for any errors or omissions in this *Accepted Manuscript* or any consequences arising from the use of any information it contains.

We were asked for materials for the table of contents, including a brief description of the significant elements of the paper. We offer the following statement: "A detailed model of DNA trapping at high fields in particle-based sieves is developed, identifying di-electrophoresis as the primary cause."



# Mechanism of DNA Trapping in Nanoporous Structures during Asymmetric Pulsed-Field Electrophoresis

Ya Zhou<sup>1</sup>, Huiying Sheng<sup>1</sup> and D. Jed Harrison<sup>1,2,\*</sup>

<sup>1</sup>*Department of Chemistry, University of Alberta, Edmonton, AB, Canada*

<sup>2</sup>*National Institute for Nanotechnology, Edmonton, AB, Canada*

## Abstract

We investigate the trapping mechanism of individual DNA molecules in ordered nanoporous structures generated by crystalline particle arrays. Two requisites for trapping are revealed by the dynamics of single trapped DNA, fully-stretched U/J shapes and hernia formation. The experimental results show there is a stronger possibility for hernias to lead the reorientation upon switching directions of the voltage at high field strengths, where trapping occurs. Fully stretched DNA has longer unhooking times than expected by a classic rope-on-pulley model. We propose a dielectrophoretic (DEP) force reduces the mobility of segments at the apex of the U or J, where field gradients are highest, based on simulations and observations of the trapping force dependence on field strength. A modified model for unhooking time is obtained after the DEP force is introduced. The new model explains the unhooking time data by predicting an infinite trapping time when the ratio of arm length differences (of the U or J) to molecule length  $\Delta X/L < \beta$ , where  $\beta$  is a DEP parameter that is found to strongly increase with electric field. The DNA polarizability calculated with the DEP model and experimental value of  $\beta$  is of the same magnitude of reported value. The results indicate the tension at the apex of U/J shape DNA is the primary reason for DNA trapping during pulsed field separation, instead of hernias.

## Introduction

The separation of megabase DNA in pulsed-field gel electrophoresis (PFGE) consumes more than 24 h, because the electric field is limited to 10 V/cm or less.<sup>1-3</sup> As field strength is increased, DNA is trapped in the sieving matrix, causing smearing of DNA bands.<sup>4</sup> Asymmetric pulsed field electrophoresis (APFE) in microfabricated artificial gels, such as nanopost arrays and colloidal crystals, dramatically decreases the separation time of 2 kbp ~209 kbp DNA to 15 s.<sup>5-7</sup> However, we find large size linear ds-DNA (>100 kbp) are trapped by APFE in three dimensional colloidal crystalline arrays, just as they are in gels, although at higher field strength (>80 V/cm) compared to gels.

The possible mechanisms of DNA trapping in gel electrophoresis have been explored. Turmel et al discussed the trapping of large DNA in gels, in the context of how modulated pulsed field methods could be used to greatly reduce trapping.<sup>4</sup> Using a model of DNA occupying a linear tube volume, DNA trapping was attributed to local conformational “defects”, such as dense regions in the gels and the formation of hernias.<sup>4</sup> Hernias, where multiple segments of a strand attempt to act as the head of the moving chain, causing complex an convoluted shapes, have been observed by single molecule fluorescence microscopy.<sup>8,9</sup> Turmel et al also suggests that a short reverse field spike can make each segment of the molecule move backward by approximately one pore, which results in the relaxation of “defects”, detrapping DNA. Viovy proposed the trapping doesn't arise solely from the arrest of chains as discussed by Turme et al. Instead, Viovy envisions DNA is trapped in topological knots around a gel fiber<sup>10</sup>, though the dynamics of such traps have been neither studied nor observed by single molecule imaging yet. The simple U- or J-shaped configuration, or hooked DNA, which can be a stable trap in a continuous field<sup>3</sup>, is not the only factor in trapping in a pulsed-field, since the U can relax through the reorientation induced by the pulsed field. The tension at the apex of a

1  
2  
3 U-shape has been estimated<sup>3, 11</sup> and identified as arising from solid friction between DNA and the gel fiber<sup>11, 12</sup>.  
4 However, Viovy has pointed out the solid friction model fails to predict several aspects of experimental  
5 observations, such as the onset of a critical trapping voltage.<sup>13</sup>  
6  
7

8  
9 In this paper, we present experimental results from single ds-DNA molecule study that provides insight to the  
10 mechanism of DNA trapping in pulsed-field electrophoresis in three dimensional colloidal crystalline arrays.  
11 We selected ds-T4 DNA separated in a structure with  $\sim 105$  nm as a model system, for reasons outlined in the  
12 SI. Utilizing a 2-D microfluidic device with an ordered, crystalline sieving matrix of silica particles,<sup>7</sup> we  
13 find no evidence that trapping is caused by blockades in dense regions<sup>4</sup> due to the high order of these  
14 structures compared to a gel. We find that trapping starts from a hook with two fully stretched arms.  
15 Multiple segments may attempt to serve as the head for motion in the newly applied field direction, creating  
16 hernias. Hernias are a common feature of trapped DNA, confounding the intended ratchet motion wherein  
17 only apex segments lead the molecular reorientation.<sup>14</sup> Our results demonstrate that at higher electric field,  
18 there is a higher probability of forming these hernias. We also find that the unhooking time of U/J shaped  
19 DNA is much longer than expected from a simple rope-on-pulley model, even after confinement by a  
20 nanoporous structure has been taken into account. The pinning at the apex of U/J is not simply due to the  
21 symmetric arm lengths. We present a modified unhooking time model which suggests the reduced mobility  
22 of DNA segments at an apex arises from a trapping force localized at the apex, yielding more fully-stretched  
23 DNA and near-apex hernias. We assign this trapping force to dielectrophoretic (DEP) forces in the tight  
24 confines of the pores, noting that the magnitude and field dependence of trapping observed is consistent with  
25 the DEP force model. Differing from DEP trapping of biomolecules in ordered microfabricated structure in  
26 other applications,<sup>15-19</sup> the critical field strength and frequency for DNA trapping in pulsed-field  
27 electrophoresis is much lower, which we attribute to the participation of hernias. The mechanism proposed  
28 in this paper also explains why reverse voltage spikes in the pulse sequence can reduce DNA trapping in both  
29 gel<sup>4, 20</sup> and crystalline arrays.  
30  
31  
32  
33  
34  
35  
36  
37

### 38 Experimental

39 DNA electrophoresis is conducted in a 2D PDMS chip (Fig. 1a). The fabrication follows Y. Zeng's method.<sup>7</sup>  
40 The separation bed and channels are filled with self-assembled arrays of 690 nm silica particles (Bangs  
41 Laboratories, Fig. 1c) constructing a nanoporous structure with 105 nm pore diameter. T4 DNA (166kbp,  
42 Wako) are stained with YOYO-1 (Invitrogen) at a ratio of 1 dye molecule to 10 base pairs. Loading buffer is  
43 4x TBE with 4%  $\beta$ -mercaptoethanol to suppress photobleaching.  
44

45 To examine the macroscopic behavior of DNA trapping at high field, a plug of T4 DNA (30ng/ $\mu$ L) is injected  
46 into the separation bed with 10 V/cm DC field. After the first few of DNA reaches at the separation bed,  
47 asymmetric pulsed fields  $E_1$  and  $E_2$  (Fig. 1b) are applied to deflect DNA stream (Fig. 1b). The angle between  
48 pulsed fields is  $135^\circ$  and  $E_1 = \sqrt{2}E_2$ . Injection DC field is turned off one minute later. The trace of the  
49 deflection band is visualized with epi-fluorescence microscope (Olympus 4X and 10X objective). The  
50 captured image stacks are processed with ImageJ. As shown in Figure 1b, the intensity of T4 DNA deflection  
51 band over time is measured at 0.54 downstream (white dash line). The dynamics of individual DNA molecules  
52 under APFE is studied on TIRF (Nikon Eclipse TiE) using a 60x oil immersion objective (Nikon). The space  
53 resolution is 0.24  $\mu$ m per pixel, as determined by calibration with a standard. The videos are captured by CCD  
54 camera (Photometrics QuantEM:512SC) at 30 frames per second in overlap mode and processed by  
55 NIS-Element. All the compressed time-laps videos in the supporting lists are speeded up or slowed down,  
56 but the real acquisition time is shown in the videos. The trapping of molecules was analyzed frame by  
57  
58  
59  
60

1  
2  
3  
4  
5  
6  
7  
8  
9  
10  
11  
12  
13  
14  
15  
16  
17  
18  
19  
20  
21  
22  
23  
24  
25  
26  
27  
28  
29  
30  
31  
32  
33  
34  
35  
36  
37  
38  
39  
40  
41  
42  
43  
44  
45  
46  
47  
48  
49  
50  
51  
52  
53  
54  
55  
56  
57  
58  
59  
60

frame.

Lengths of hooked DNA were measured, and those in the range of 55 to 65  $\mu\text{m}$  observed length were evaluated using the rope on pulley model. At 202.2 V/cm, our measured contour length is  $62 \pm 2 \mu\text{m}$ . (The true contour length of unlabeled T4 DNA is 55.8  $\mu\text{m}$ , with an observed length for fluorescence detection of the labeled molecule ranging from 60 to 65  $\mu\text{m}$ .<sup>21, 22</sup>) For analysis,  $t = \text{zero}$  was established at the time where no coiling was visible on the shorter segment, and the total length lay within the stated range above.

## Results and Discussions

### 1. Macroscopic behaviors of T4 DNA trapping

Without trapping, the motion of DNA in APFE should follow a ratchet model,<sup>6, 23, 24</sup> wherein a DNA stream or plug migrates vertically while being deflected at a certain angle (Fig. 2a-2c). As the voltage switches, the head and tail of the stretched DNA switch roles, leading to angular dispersion dependent upon size, when conditions are appropriate for the model to apply. However, trapping large DNA at higher fields does occur within the nanoporous particle lattice. In Figure 2c, an injection plug of DNA is formed by turning off the voltage on the injection channel after a brief injection, while retaining voltage in the separation bed. The snapshot (Fig. 2d), taken 7 min later, shows that instead of moving out of the view field, part of the DNA plug is trapped in the nanoporous structure. Figure 2e shows the intensity profile of the pixels along the arrow in Figure 2d, indicating DNA molecules are trapped.

DNA trapping in a porous crystalline lattice of particles occurs when the field strength is beyond a critical value,  $E_{\text{crit}}$ . Figure 3 shows the intensities of a T4 DNA deflection band over time. The intensities are extracted from the maximum intensities in each frame. At  $E_2=71.4 \text{ V/cm}$ , DNA molecules migrate through the bed without being trapped, showing a sharper band in Figure 3a, while they are partially trapped at 114.3 V/cm and 142.9 V/cm, giving broad bands. The trapping in a particle-based lattice follows the same trend as in a gel<sup>4, 10</sup>, except that  $E_{\text{crit}}$  is much higher than that in gel, leading to more rapid separations.

DNA trapping is reduced when reverse spikes  $E_1^*$  and  $E_2^*$  are inserted into the two primary pulsed fields (Fig. 3b). A reverse spike, applied in the opposite direction with half the magnitude, follows each forward pulse, using the parameters given in Table 1. As expected, the apparent mobility is decreased by the reverse spikes. The effect of reverse spikes on a single DNA molecule is illustrated by TIRF videos F1 and F2 in the supporting information, which compare results without and with the spikes, respectively. The electric fields applied in videos F1 and F2 are the same as those for the black and red curves in Figure 3b, correspondingly. Without reverse spikes, DNA molecules are trapped by high electric field ( $E_2=142.9 \text{ V/cm}$ ) at the end of video F1, while the molecules are not trapped in video F2. The importance of the effect of reverse spikes on understanding trapping is further explored below.

### 2. Dynamics of single DNA trapping and the Role of Hernias

Single molecule observations capture the dynamics of DNA trapping in crystalline sieves, as illustrated in Fig. 4 and Video F3. As a first step the molecule hooks around a silica particle and is stretched (Fig. 4a), then after the field switches to  $E_2$ , hernias form and grow, with various segments vying to act as the head of the molecule (Fig. 4b). The molecule does not move as predicted by the ratchet model, and ends up trapped in the matrix (Fig. 4c). We note that these effects are field dependent, and do not occur at lower fields, such as 71.4 V/cm, ruling out adsorptive interactions with the silica as a primary cause. Additionally, the 4x TBE buffer was selected to reduce electroosmotic flow and zeta potential of the silica, which reduces DNA-silica interactions.

1  
2  
3  
4  
5 Apart from the field strength, the length of a hernia also depends on DNA conformation, as part of a molecule  
6 may be coiled before it is reoriented by the electric field, and the coiled segments are more favorably disposed  
7 to form hernias than the stretched part. The formation of a hernia from a coiled region is commonly referred  
8 to as leakage from the tube model for DNA. Fortunately, the results of the reverse spike experiments offer a  
9 route to simplify the analysis of trapping. When reverse spikes are inserted into the two primary pulsed  
10 fields, DNA molecules are not trapped, as the fully stretched U-shapes are relaxed and released. A similar  
11 result is observed when the field is intermittently interrupted at the same frequency as used for reverse spikes.  
12 A trapped, partially relaxed molecule will either become fully stretched, or the relaxed state will lead to  
13 release and de-trapping, as evidenced in the section below. We infer that being fully-stretched can be treated  
14 as a requisite for the trapping, so that our analysis can be confined to the study of fully stretched DNA.  
15  
16  
17  
18

19  
20 The influence of hernias on DNA trapping at different fields is shown in Figure 5. According to the ratchet  
21 model, it is the apex segments that lead the reorientation of hooked DNA, and for the DNA shown in Figure  
22 5a, the hernias are segments  $h_1$  and  $h_2$ . The length of a hernia as it grows from an individual fully stretched  
23 U-shaped molecule is plotted as a function of time (Fig. 5), once the field is switched to  $E_2$ . The results  
24 show at low fields the hernias tend to shorten and often are extinguished over time, while at higher electric  
25 fields, the hernias are longer in duration and in physical length. Thus, there is a higher probability of  
26 forming hernias and those hernias have a greater chance to be substantially stretched, trapping the molecule,  
27 when fields are higher. Hernias are very common in pulsed-field electrophoresis in general, and their lengths  
28 are theoretically predicted to increase with electric field,<sup>25, 26</sup> consistent with our results in the crystalline  
29 sieves.  
30  
31  
32  
33

34  
35 The data in Figure 5 are extracted from 0.2 Hz APFE experiments, in which the duration time of each pulse is  
36 longer than the reorientation time. This pulse period is long enough that the field strength is the physically  
37 dominant variable for the study of hernias, allowing evaluation of the formation, stretching and elimination  
38 from an initially fully-stretched U/J shape. The trapping dynamics are followed for molecules transitioning  
39 from the free state, to the U/J hooked state, and then into hernia formation and evolution. The results show  
40 0.5 s is a watershed for the growth of hernias at high field, as many hernias are eliminated at this point.  
41 Surviving hernias beyond 0.5 s are substantially stretched and lead the reorientation when the field switches,  
42 instead of the apex segments. For the same electric field, hernia evolution is cut short as a result of the  
43 shorter pulse durations at higher frequencies, as suggested by the red lines in Figure 5c. For example, at 2  
44 Hz, most of the dangling hernias like  $h_2$  will not be eliminated during the reorientation and may cause trapping.  
45 Video F4 in the supporting material shows DNA trapped at 0.5 Hz ( $E_2=142.9$  V/cm). When compared to the  
46 conformation of trapped DNA at 2 Hz (Fig. 4c, video F3), it is clear that at 0.5 Hz the DNA only loses its  
47 mobility at the apex, with the two arms still shuttling through nanopores under the pulsed-fields. Notably, it  
48 is hernias near the apex location that tend to become extended and trapped, as no distant hernias survive after  
49 ~ 600 ms; all long lived hernias reside in the near apex region, as indicated in Figure 5d. This observation is  
50 significant given that those near-apex hernia segments, like  $h_1$  in Figure 5a, clearly exhibit comparable or  
51 larger mobility than the apex segments, and attempt to act as the head of a molecule after the electric field  
52 switches. (see Supplemental Figure S1).  
53  
54  
55  
56  
57

58  
59 It is clear from our data that trapping of the apex itself is a significant feature of the trapping phenomenon,  
60 even though the formation of hernias is a more visually obvious trapping characteristic. This conclusion is  
further supported by the fact that reverse spikes reduce trapping, even though these spikes can actually

increase the rate of hernia formation through forming more coiled segments via DNA relaxation. Taken with the results presented below, and in Figure 5c-5d for high fields it is evident that long lived hernias are generated as a result of affects near the pinned apex state, not from tube leaks generated from coiled segment lengths or other defects. We conclude that hooking is the primary requisite for trapping, and that hernias, while appearing significant in causing trapping are actually a consequence of the hooks that are the primary source of trapping.

### 3. Role of hooking

Hooking has also been recognized as playing a role in trapping DNA. The U/J shaped hook, and the time to release this hook, has been described by a rope-on-pulley model.<sup>27, 28</sup> However, unhooking times observed at fields where trapping occurs are much longer than predicted by the rope-on-pulley model. Video F5 shows a J-shaped DNA that can not be unhooked under high electric field ( $E_1=202$  V/cm). We propose that the same affect accounts for the decreased mobility seen at the apex of herniated DNA, discussed above.

We measured the unhooking time of fully-stretched U/J shaped DNA in crystalline sieves and compared the results with an unhooking time model<sup>29</sup>:

$$t_{unhook} = -\frac{L}{2\mu E} \ln\left(1 - \frac{2x_1}{L}\right) \quad (1)$$

which is derived from the rope-on-pulley model. In Equation 1,  $L=55.8$   $\mu\text{m}$  is the contour length of T4 DNA and  $x_1$  is the length of short arm (Fig. 6a). The model was initially proposed to describe the unhooking dynamic after DNA collides with a single post in free solution. To apply Equation 1 to the nanoporous structure, we retain a rope-on-pulley model, but account for strong restrictions of motion in this confined structure, by replacing the free solution mobility  $\mu_0$  with  $\mu$ , the mobility of confined DNA. Mobility  $\mu$  can not be directly obtained by measuring the DNA migration time, because DNA molecules frequently collide with silica particles and transform among different conformations, slowing down the migration rate. In free solution and the situation in which a polyelectrolyte is fully stretched by strong field, we use a local force picture that the frictional force is equivalent to the electric field force, giving:

$$\xi\mu E = Eq_{\text{eff}} \quad (2)$$

where  $q_{\text{eff}}$  is the effective charge of DNA. Equation 2 is generally applied to the ideal unhooking of U/J at high field.<sup>29, 30</sup> We assume  $q_{\text{eff}}$  of T4 DNA does not change with DNA conformation. Therefore, according to Equation 2, mobility is inversely proportional to the friction coefficient

$$\frac{\mu}{\mu_0} = \frac{\xi_0}{\xi} \quad (3)$$

The friction coefficient in free solution is<sup>31</sup>

$$\xi_0 = 6\pi\eta g_r \quad (4)$$

With equation 2 and 4, we calculate  $q_{\text{eff}} = 0.034$  electrons per base pair (see SI), consistent with the value obtained by Smith<sup>32</sup>. Because the pore diameter in crystalline sieves is about 105 nm, twice the DNA persistence length (50 nm), the DNA confined in the nanoporous structure falls into Odijk's regime, leading to a friction coefficient<sup>33, 34</sup>

$$\xi = \frac{2\pi\eta L}{\ln(4D/\pi w)} \quad (5)$$

Substituting Equation 4 and 5 into Equation 3, with radius of gyration  $g_r = 1.31 \mu\text{m}^{35}$ , pore diameter  $D = 105$  nm and diameter of DNA  $w = 2.4$  nm, we get  $\mu = 0.279 \mu_0$ . The measured free solution mobility  $\mu_0$  of DNA in 4x TBE buffer is  $(3.175 \pm 0.059) \times 10^{-8} \text{ m}^2/(\text{V} \cdot \text{s})$ .

After rewriting the mobility, the theoretical unhooking time (solid curves in Fig. 6b-6d) can fit most experimental values (dots) at low field ( $E_2=74.1$  V/cm). The unhooking time was measured as starting when the short arm was fully-stretched under the pulse  $E_1$ , not from the initial collision. At this point in time, given the high field strength and confining pore structure, the long arm of a hook is highly extended. As field strength is increased, the experimental values deviate from the theoretical plots. At higher fields, some U/J shape molecules are pinned at the apex, showing infinite unhooking time. Experimentally, unhooking times longer than 1.5 s at  $E_2=74.1$  V/cm and those longer than 1 s at  $E_2=114.3$  and 142.9 V/cm are taken as infinite, and plotted as red dots in Figure 6.

Based on the experimental unhooking time data, we propose there is an external force other than electrophoretic force acting on the apex segments and resisting the rope-on-pulley motion. Randall et al. gave the equations of motion of two arms in the simple rope-on-pulley model<sup>29</sup>

$$j\xi \left( \frac{dx_1}{dt} - \mu E \right) = -T \quad (6a)$$

$$(N - j)\xi \left( \frac{dx_2}{dt} - \mu E \right) = -T \quad (6b)$$

where  $j$  is the number of base pairs on the short arm,  $N=166$  kbp for T4 DNA, and  $T$  is the intramolecule tension connecting the short arm and the long arm at the apex. Assuming there is an external force  $F_{ext}$  at the apex, Equation 6a is changed to

$$j\xi \left( \frac{dx_1}{dt} - \mu E \right) = -T + F_{ext} \quad (6c)$$

$F_{ext}$  resists the short arm sliding over the hooking spot while it is stretched by electrophoretic force, which results in more fully-stretched DNA. As described in the paper by Randall et al., the unhooking time can be solved by integrating the difference of Equation 6b and 6c, using  $dx_1/dt = dx_2/dt$  and  $j/N = x_1/L$ :

$$t_{unhook} = -\frac{L}{2\mu E} \ln \left( 1 - \frac{1}{1-\beta} \frac{2x_1}{L} \right) \quad (7)$$

In Equation 7, the newly defined parameter

$$\beta = F_{ext}/\xi\mu E \quad (8)$$

The new unhooking time model requires  $1 - 2x_1/(1-\beta)L > 0$ , predicting that unhooking is only possible when the length difference of two arms  $\Delta x > \beta L$ . Otherwise, the unhooking time is infinite.

The value of  $\beta$  can be obtained from the critical condition  $\Delta x = \beta L$ . The critical  $\Delta x$  of each subplot from Figure 6b to 6d is determined by the leftmost red dot, using  $L = 2x_1 + \Delta x$ . The dashed lines in Figure 6 are plots of Equation 7. The two unhooking time models form the left and right bounds of a 2D value domain for experimental values at different electric fields. The solid dots in Figure 6 are collected from a complete sample, which reflects the real distribution of unhooking times of substantially stretched U/J at different fields. A second data set, shown as hollow dots, was collected, focusing on shorter value of  $x_1$  to ensure the accuracy of  $\beta$  and test the new model.

#### 4. Dielectrophoretic trapping

We propose the source of  $F_{\text{ext}}$  is a dielectrophoretic (DEP) force. Figure 6e shows the scaling relation between  $\beta$  and field strength is  $\beta \sim E^2$ , suggesting  $F_{\text{ext}}$  must quickly increase with  $E$  (Eq. 8). In a non-uniform electric field, polarizable molecules are subjected to a DEP force  $F_{\text{DEP}}$ :

$$F_{\text{DEP}} = \alpha \nabla |E|^2 \quad (9)$$

where  $\alpha$  is molecule polarizability.<sup>18,36</sup> The electric field in the separation bed is non-uniform, owing to the different permittivity's and conductivities of 4x TBE buffer and silica particles. Simulation results (Fig. 7 and Fig. S3) show both the electric field strength  $E$  and the field gradient  $\nabla |E|^2$  are significantly higher at the contact zone of two particles whose inner tangent is not perpendicular to the field direction. The electrophoretic force on the two arms of U/J molecules presses the apex segments close to the particle where  $E$  and  $\nabla |E|^2$  are higher in comparison to the pore, and the positive DEP force traps apex segments at the high field strength region, resisting unhooking.  $\nabla |E|^2$  is relatively small at other possible hooking spots on the particle surface. Therefore,  $F_{\text{DEP}}$  is variable at different hooking spots, just as is parameter  $\beta$ . We correlate the dashed lines in Figure 6 with the unhooking time model applicable at the highest field gradient areas shown in red in Figure 7, while DNA hooked at the lower field gradient, blue, areas have shorter unhooking time with a smaller  $\beta$ . This interpretation explains the scattered distribution of experimental values, lying in a range between the extreme trapping of the maximum value of  $\beta$  and that of the original rope-on-pulley model with a  $\beta$  of zero.

Using the assumption that a DEP force is the external force at the apex, we calculate the T4 DNA polarizability  $\alpha = \beta \xi \mu E / \nabla |E|^2$  by substituting Equation 9 into Equation 8. At  $E_2 = 142.9$  V/cm, where trapping is obvious, we calculate  $\alpha = 1.31 \times 10^{-29} \text{ Fm}^2$ , using  $\beta = 0.216$  which is obtained from the unhooking time experiment (Fig. 6d),  $\xi \mu = 6\pi\eta g_r \mu_0$  (Eq. 3 and 4) with viscosity  $\eta = 1.16$  cP<sup>37</sup>,  $E = E_1 = 202.1$  V/cm and the maximum field gradient  $\nabla |E|^2 = 3.04 \times 10^{17} \text{ mkg}^2/(\text{s}^6\text{A}^2)$  at the contact area of two particles (supplemental Fig. S4). The calculated DNA polarizability is of the same magnitude of the reported value<sup>38</sup>, strongly supporting our DEP force model.

There are two other possible external forces, hydrodynamic friction and solid friction. In unhooking time models, hydrodynamic friction is already included through the mobility  $\mu$ , and can not lead to infinite unhooking times according to Equation 7. Burlastky et al. proposed solid friction between DNA and gel.<sup>12</sup> Assuming the friction coefficient is  $\mu_f$  and substituting  $F_{\text{ext}} = \mu_f E q_{\text{eff}}$  into the definition formula of  $\beta$ , the parameter  $\beta = \mu_f q_{\text{eff}} / \mu \xi$  becomes field independent, in contrast to the observed scaling relation. Interaction between DNA and the electrical double layer at the silica interface is another potential source of an external force. For the buffer used here, the Debye length is 0.743 nm, which is substantially smaller than the region of high external field gradient that can generate a DEP force.

From Equation 2, we obtain  $\beta = F_{\text{ext}} / \xi \mu E = F_{\text{DEP}} / F_{\text{EP}}$ . The physical meaning of parameter  $\beta$  is the ratio of DEP force at the apex to the electrophoretic force on the entire DNA molecule. The calculated values of  $\beta_{\text{max}}$  at different field strength are much smaller than 1, indicating that the DEP force is a modest perturbation on DNA electrophoresis. The dominant force in APFE experiments remains electrophoretic force, so the DNA plug can migrate downwards in Figure 2. However, at higher fields, the mobility of apex segments is reduced due to the presence of a positive DEP force, and the molecule becomes pinned, forming U/J shaped hooks. Pinning at the apex then results in near-apex hernias, arising from the attempted reorientation of the molecules when the potential switches to create a ratchet and the apex can not respond, so another portion of the molecule acts as the head, further compounding the trap for the DNA. Reverse spikes inserted within a given field direction of APFE dislodges the molecules from the high  $F_{\text{DEP}}$  zone, either directly, or through sufficient relaxation and recoil to mobilize away from the apex region, thus reducing trapping (video F6).

## Conclusion

We reveal the primary mechanism of DNA trapping in colloidal crystal during pulsed-field electrophoresis is due to hooking, and show this is consistent with a dielectrophoretic trapping force. We have shown that as the field strength is increased, the magnitude of trapping force increases with a field dependence consistent with dielectrophoretic forces. Modeling of the electric field and field gradient at the contact zone of the particles shows the dielectrophoretic force available increases much faster than the electrophoretic force. Using the calculated force from dielectrophoresis and the observed trapping force provides an estimate of the polarizability of the molecule that is in agreement with literature values. At lower frequency ( $< 1$  Hz), the pinning of DNA at the apex of a hook to form the U/J shape is the trigger of trapping, followed by extended stretching of the DNA. Hernias are then formed, as other segments of the molecule attempt to become the head instead of the immobile apex, when the field direction is switched. These hernias can become permanent and compound the strength of the trap. At higher frequency (2 Hz), hernias appear to cause the trapping of T4 DNA, because the following reorientation takes place while the apex segments and hernias are competing to act as head. However, the near apex hernias tend to dominate over time, and it is clear these form because of pinning of the apex, again illustrating that trapping at the apex is the initial trigger for irreversible trapping.

The trapping mechanisms discussed for gels are more varied than those we report here for a particle-based sieve structure. Trapping in the particle beds is readily understood in terms of macroscopic forces (DEP) and polymer dynamics, in contrast to DNA trapping in gels. As discussed in the introduction, a friction force at the hooking intersection of DNA and gel strand has been invoked, but the model does not describe all of the experimental results, yet evidence that pinning at the origin of the hook for a U-shape does exist. In the particle matrix, the macroscopic dielectrophoretic force does explain the importance of hooking in trapping of DNA. In both gels and in the particle sieves investigated here, the effect of reverse spikes in the field is to relax the DNA strands and allow them, or encourage them, to mobilize away from the apex trapping points associated with hooks. In the case of the particle sieves the mechanism of trapping by hooking can clearly be linked with dielectrophoresis, while it remains partly obscured in gels.

The model proposed here is applicable to linear ds-DNA. Insulator-based dielectrophoresis (iDEP) trapping of single strand DNA and supercoiled plasmid DNA has been reported by several groups, confirming that similar forces will be at play with those materials. However, to apply the model we have developed, one would have to take into account how the polymer physics changes for these forms of DNA relative to the linear, ds-DNA studied here.

## Acknowledgment

The work was supported by grant from Natural Sciences and Engineering Research Council of Canada (NSERC) and the National Institute for Nanotechnology (NINT).

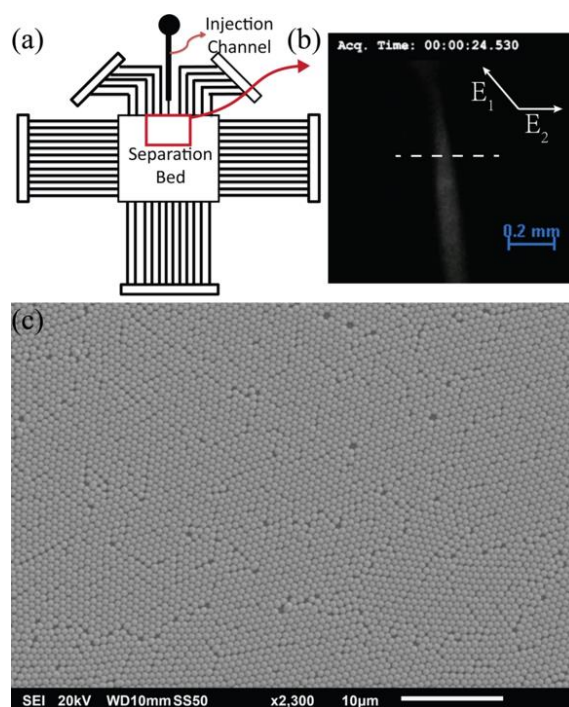


Figure 1: (a) Schematic of the microchip for DNA separation. The separation bed and microchannels are filled with a colloidal crystal of silica particles, except for the injection channel. (b) Fluorescence micrograph (4X objective) of deflection band of a T4 DNA plug under asymmetric pulsed field electrophoresis (APFE).  $E_1$  and  $E_2$  are two square pulses in APFE.  $E_1 = \sqrt{2} E_2$ . Frequency is 0.5 Hz. The dashed line represents the position for measuring fluorescent intensity. (c) SEM image of the crystalline silica (690 nm diameter) in the separation bed.

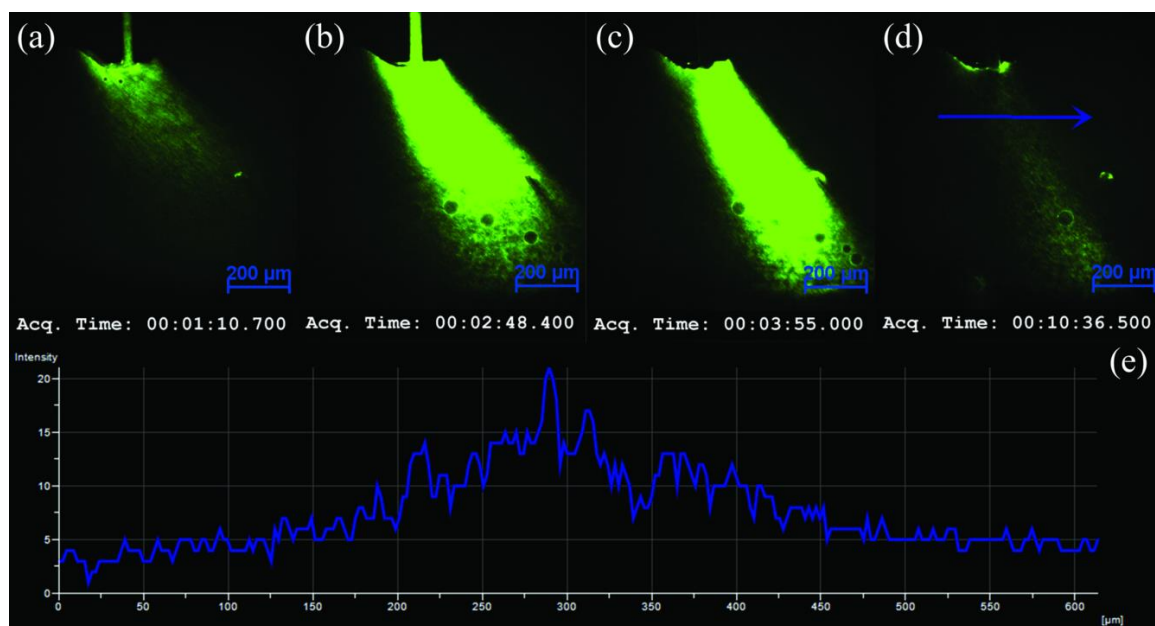


Figure 2: (a-d) Migration of a T4 DNA plug in the separation bed captured by fluorescence microscope (10X objective). The field strengths of asymmetric pulsed-fields  $E_1$  and  $E_2$  are 202.0 V/cm and 142.9 V/cm, respectively, with 0.5 Hz frequency. The time trace starts at the beginning of 2D separation. In (c), continuous injection was stopped, creating an empty injection channel and a plug of injected material. (e) The intensity profile along the blue arrow in (d), showing a few of DNA are trapped in the sieves.

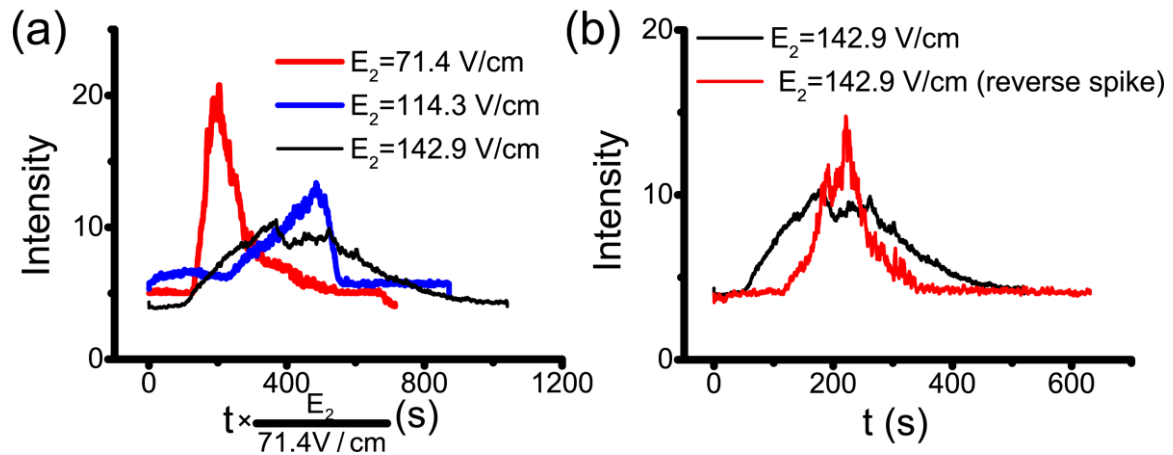


Figure 3: (a) Intensity-time curves at several fields at 0.5Hz. Intensity is measured 0.54 cm downstream (dashed line in Fig. 1b). Time is normalized by field strength. Trapped DNA causes a broad band, mobile DNA gives sharper spikes. (b) Effect of reversed spikes on DNA trapping at high electric field.  $E_2 = 142.9 \text{ V/cm}$ ,  $f = 0.5 \text{ Hz}$ . ++

 1  
2  
3  
4  
5  
6  
7  
8  
9  
10  
11  
12  
13  
14  
15  
16  
17  
18  
19  
20  
21  
22  
23  
24  
25  
26  
27  
28  
29  
30  
31  
32  
33  
34  
35  
36  
37  
38  
39  
40  
41  
42  
43  
44  
45  
46  
47  
48  
49  
50  
51  
52  
53  
54  
55  
56  
57  
58  
59  
60

Table 1 Parameters of forward pulses and reversed spikes

	$E_1$	$E_1^*$	$E_2$	$E_2^*$
direction				
Field strength (V/cm)	202.1	101.0	142.9	71.4
Duration time (s)	1.0	0.1	1.0	0.1

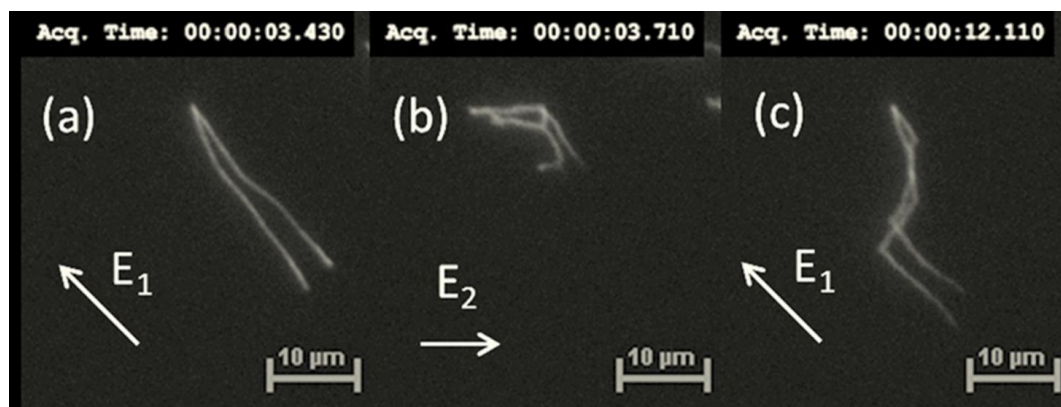


Figure 4: TIRF micrograph of a single DNA trapped in APFE.  $E_2=142.9$  V/cm,  $f=2$  Hz. (a) DNA collides with, then hooks around a silica particle. (b) Hernias forms after electric field switches. (c) The conformation of trapped DNA at 2 Hz. The process of single DNA trapped at the same field strength, but 0.5 Hz, is recorded in video F3.

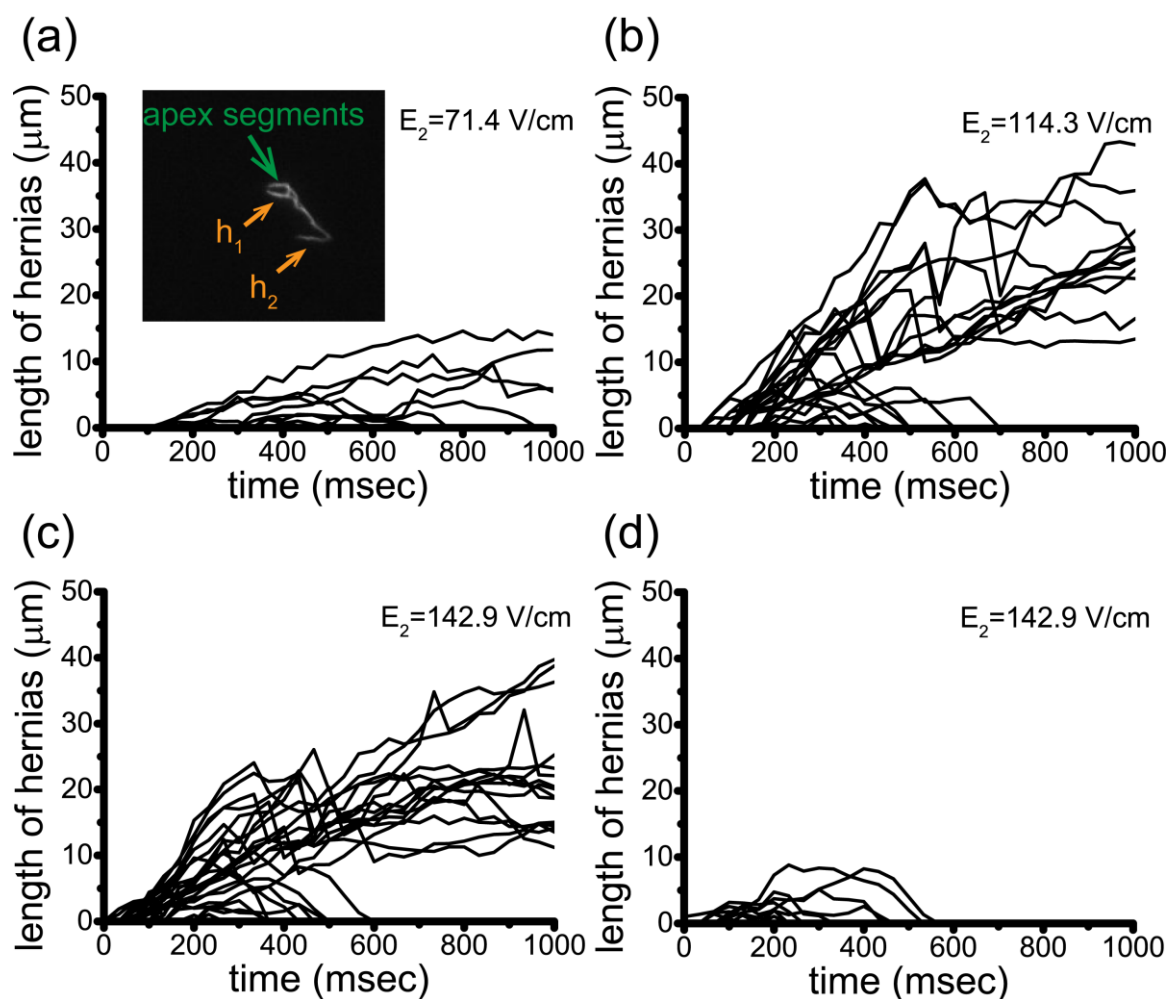


Figure 5: (a) The comb-like conformation of hernias after electric field switching. Apart from the apex segments, which should lead the molecule's reorientation according to ratchet model, other segments responding to the field are labelled as hernias. For all studied molecules, the length of hernias is measured every 33 ms after the field switches to  $E_2$ . For the molecule shown in the image, the total length of hernias =  $2h_1 + h_2$ . (a-c) The total lengths of hernias are shown as a function of time at several field strengths, with 50 molecules presented in each graph. The red lines in (c) represent the duration time of the  $E_2$  portion of the field pulse on the x-axis for the frequencies indicated. (d) 30 hernias formed at  $E_2 = 142.9$  V/cm were identified as either distant hernia or near-apex hernia (within  $2.8 \mu\text{m}$  of the apex, 5% of contour length). The evolution of distant hernias is shown in (d), indicating all the long lasting hernias in (c) are near-apex hernias. Evolution traces isolated for the near apex hernias in (c) can be found in supplemental Figure S2.

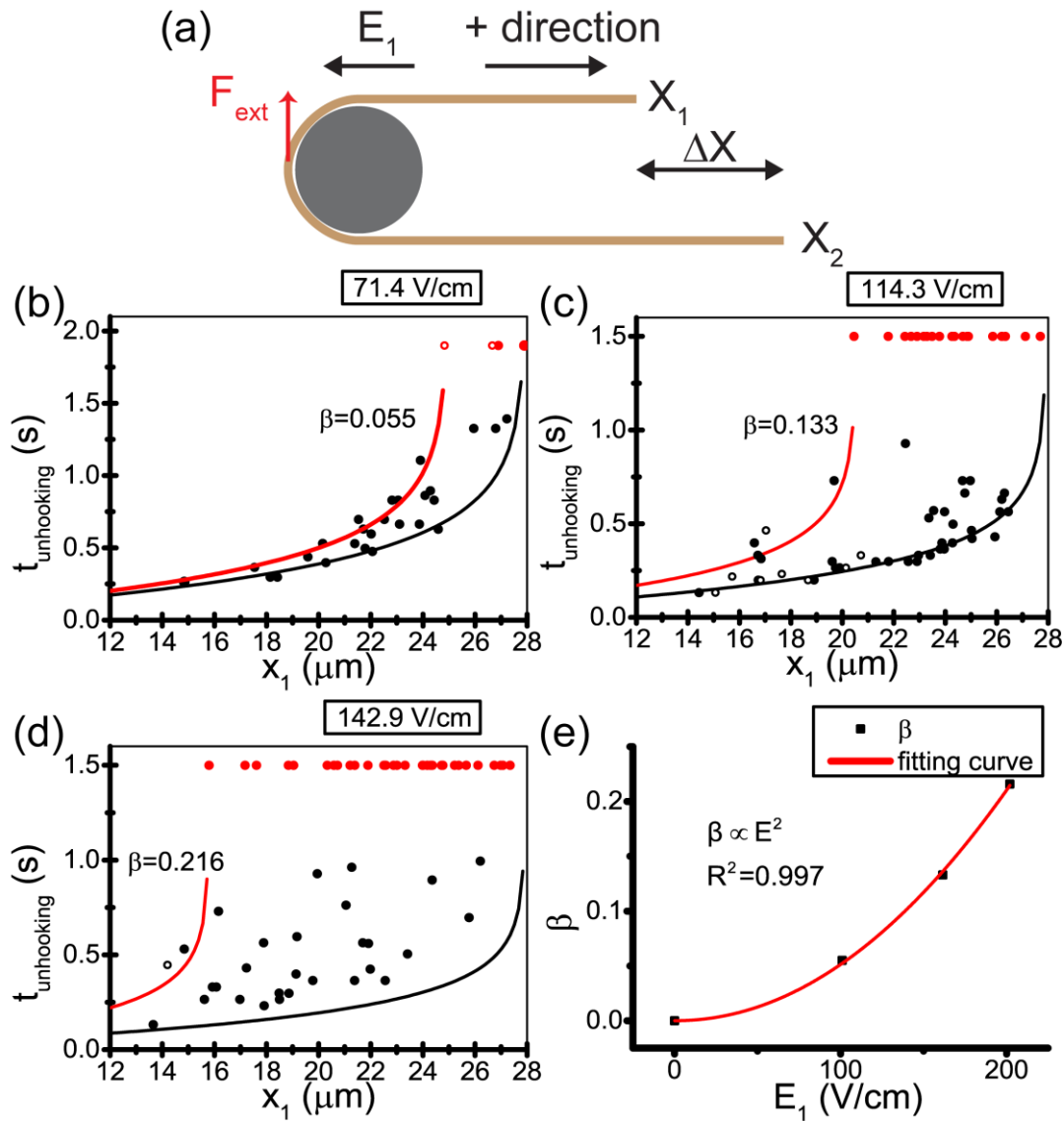


Figure 6: (a) Scheme of “rope-on-pulley” model. The negatively charged molecule should slip away from the J-shape under the external electric field  $E_1$ , due to the unequal lengths of the two arms. (b-d) Unhooking times of U/J shaped DNA at different electric fields. The solid lines follow the theoretical model of Randall et al. with  $\beta=0$ . The dashed lines follow the modified model of eq 7, for the maximum of  $\beta$  as determined at different field strengths. Dots represent experimental unhooking times. Red dots represent infinite unhooking time, appearing at 1.5 s on the y-axis. The solid dots represent the first data set which is obtained from complete sample statistics in several TIRF videos. The hollow dots represent a second data set which only focused on shorter  $x_1$ . (e) Scaling relation between dielectrophoresis parameter  $\beta$  and electric field strength.

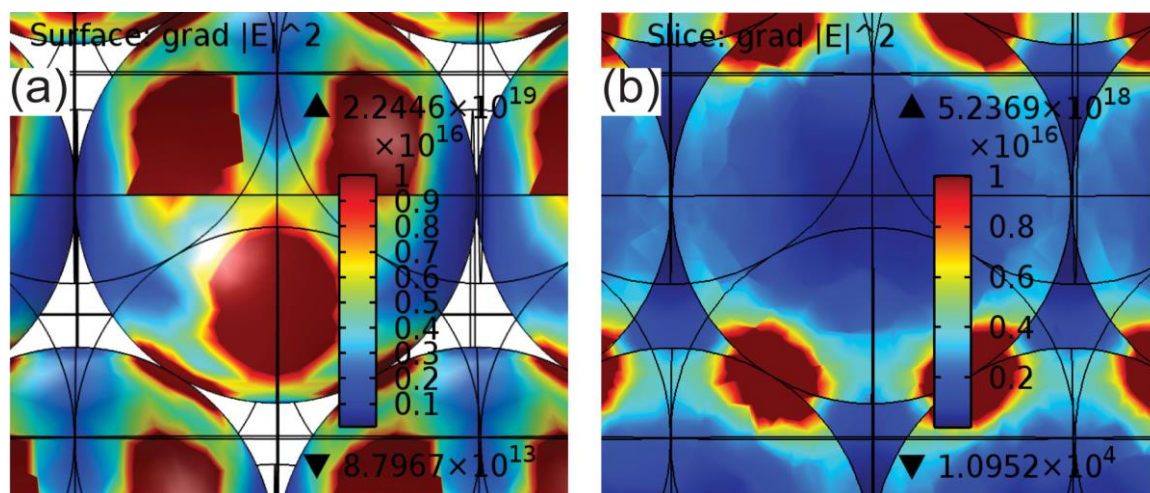


Figure 7: Simulation results of electric field gradient  $\nabla|E|^2$  in the nanoporous structure. The permittivity's of 4X TBE buffer and silica particle are  $77.232 \epsilon_0$ <sup>39</sup> and  $4.2 \epsilon_0$ , respectively. The conductivity of buffer and silica are  $0.22$  and  $1 \times 10^{-10}$  S/m, respectively. The direction of applied electric field is from left to right. Field strength  $E$  (see supplemental Figure S3) is non-uniform in the nanoporous structure. Field gradient  $\nabla|E|^2$  plotted in 2D graphs, showing (a) the gradient on the silica surface, as a projection of the upper surface onto a plane passing through the particle's centre, parallel to the direction of the field, and (b) a two-dimensional slice taken along the same plane, showing the field gradient in the pore. Red is high field gradient, blue is low.

## Reference:

1. E. M. Southern, R. Anand, W. R. A. Brown and D. S. Fletcher, *Nucleic Acids Res.*, 1987, 15, 5925-2943.
2. K. Gunderson and G. Chu, *Mol. Cell. Biol.*, 1991, 11, 3348-3354.
3. S. Gurrir, S. B. Smiths and C. Bustamante, *Proc. Natl. Acad. Sci. U.S.A.*, 1999, 96, 453-458.
4. C. Turmel, E. Brassard, G. W. Slater and J. Noolandi, *Nucleic Acids Res.*, 1990, 18, 569-575.
5. W. D. Volkmuth and R. H. Austin, *Nature*, 1992, 358, 600-602.
6. L. R. Huang, J. O. Tegenfeldt, J. J. Kraeft, J. C. Sturm, R. H. Austin and E. C. Cox, *Nat. Biotechnol.*, 2002, 20, 1048-1051.
7. Y. Zeng, M. He and D. J. Harrison, *Angew. Chem. Int. Ed.*, 2008, 47, 6388-6391.
8. D. C. Schwartz and M. Koval, *Nature*, 1989, 338, 520-522.
9. H. Zhang and M. J. Wirth, *Anal. Chem.*, 2005, 77, 1237-1242.
10. J.-L. Viovy, F. Miomandre, M.-C. Miquel, F. Caron and F. Sor, *Electrophoresis*, 1992, 13, 1-6.
11. D. Stigter, *Macromolecules*, 2000, 33, 8878-8889.
12. S. Burlatsky and J. Deutch, *Science*, 1993, 260, 1782-1784.
13. J.-L. Viovy, T. Duke, S. Burlatsky and J. Deutch, *Science*, 1994, 264, 112-113.
14. T. A. J. Duke, R. H. Austin, E. C. Cox and S. S. Chad, *Electrophoresis*, 1996, 17, 1075-1079.
15. S. K. Srivastava, A. Gencoglu and A. R. Minerick, *Anal. Bioanal. Chem.*, 2011, 399, 301-321.
16. B. H. Lapizco-Encinas, B. A. Simmons, E. B. Cummings and Y. Fintschenko, *Anal. Chem.*, 2004, 76, 1571-1579.
17. R. C. Gallo-Villanueva, C. E. Rodriguez-Lopez, R. I. Diaz-de-la-Garza, C. Reyes-Betanzo and B. H. Lapizco-Encinas, *Electrophoresis*, 2009, 30, 4195-4205.
18. C.-F. Chou, J. O. Tegenfeldt, O. Bakajin, S. S. Chan, E. C. Cox, N. Darnton, T. Duke and R. H. Austin, *Biophys. J.*, 2002, 83, 2170-2179.
19. F. Camacho-Alanis, L. Gan and A. Ros, *Sensors and Actuators B*, 2012, 173, 668-675.
20. C. Bustamante, S. Gurrieri and S. B. Smith, *Trends Biotechnol.*, 1993, 11, 23-30.
21. T. T. Perkins, D. E. Smith, R. G. Larson and S. Chu, *Science*, 1995, 268, 83-87.
22. O. B. Bakajin, T. A. J. Duke, C. F. Chou, S. S. Chan, R. H. Austin and E. C. Cox, *Phys. Rev. Lett.*, 1998, 80, 2737-2740.
23. N. Nazemifard, S. Bhattacharjee, J. H. Masliyah and D. J. Harrison, *Angew. Chem. Int. Ed.*, 2010, 122, 3398-3401.
24. N. Nazemifard, S. Bhattacharjee, J. H. Masliyah and D. J. Harrison, *Electrophoresis*, 2013, 34, 2453-2463.
25. J. M. Deutsch, *Phys. Rev. Lett.*, 1987, 59, 1255-1258.
26. D. Long and J.-L. Viovy, *Physica A*, 1997, 244, 238-253.
27. J. M. Deutsch, *Science*, 1988, 240, 922-924.
28. J. M. Deutsch and T. L. Madden, *J. Chem. Phys.*, 1988, 90, 2476-2484.
29. G. C. Randall and P. S. Doyle, *Macromolecules*, 2006, 39, 7734-7745.
30. W. D. Volkmuth, T. Duke, M. C. Wu, R. H. Austin and A. Szabo, *Phys. Rev. Lett.*, 1994, 72, 2117-2120.
31. P.-G. de Gennes, *Scaling Concepts in Polymer Physics*, Cornell University Press, 1979.
32. S. B. Smith and A. J. Bendich, *Biopolymers*, 1990, 29, 1167-1173.

- 1  
2  
3  
4 33. D. C. Morse, *Macromolecules*, 1998, 31, 7044-7067.  
5 34. W. Reisner, K. J. Morton, R. Riehn, Y. M. Wang, Z. Yu, M. Rosen, J. C. Sturm, S. Y. Chou, E. Frey  
6 and R. H. Austin, *Phys. Rev. Lett.*, 2005, 94, 196101.  
7 35. J. Tang, N. Du and P. S. Doyle, *Proc. Natl. Acad. Sci. U.S.A.*, 2011, 108, 16153-16158.  
8 36. T. B. Jones, *Electromechanics of Particles*, Cambridge University Press, 1995.  
9 37. C.-C. Hsieh, A. Balducci and P. S. Doyle, *Nano Lett.*, 2008, 8, 1683-1688.  
10 38. J. Regtmeier, R. Eichhorn, L. Bogunovic, A. Ros and D. Anselmetti, *Anal. Chem.*, 2010, 82,  
11 7141-7149.  
12 39. S.-S. Hsieh, H.-C. Lin and C.-Y. Lin, *Colloid. Polym. Sci.*, 2006, 284, 1275-1286.  
13  
14  
15  
16  
17  
18  
19  
20  
21  
22  
23  
24  
25  
26  
27  
28  
29  
30  
31  
32  
33  
34  
35  
36  
37  
38  
39  
40  
41  
42  
43  
44  
45  
46  
47  
48  
49  
50  
51  
52  
53  
54  
55  
56  
57  
58  
59  
60